Supplementary Information

Aramid nanofiber-poly(vinyl alcohol) composite gel polymer electrolytes for lithium chloride-based supercapacitors

Yuseung Choi [a,†], Gilyong Shin [a, b,†], Eun Jae Nam [a], Ji Heon Hong [a], Byeong Jun So [a], and Tae June Kang [a,]*

[a] Department of Mechanical Engineering, Inha University, Incheon 22212, South Korea

[b] Department of Aeronautics and Astronautics, Stanford University, Stanford, CA 94305, United States

† These authors contributed equally.

*Corresponding authors: Tae June Kang (tjkang@inha.ac.kr)

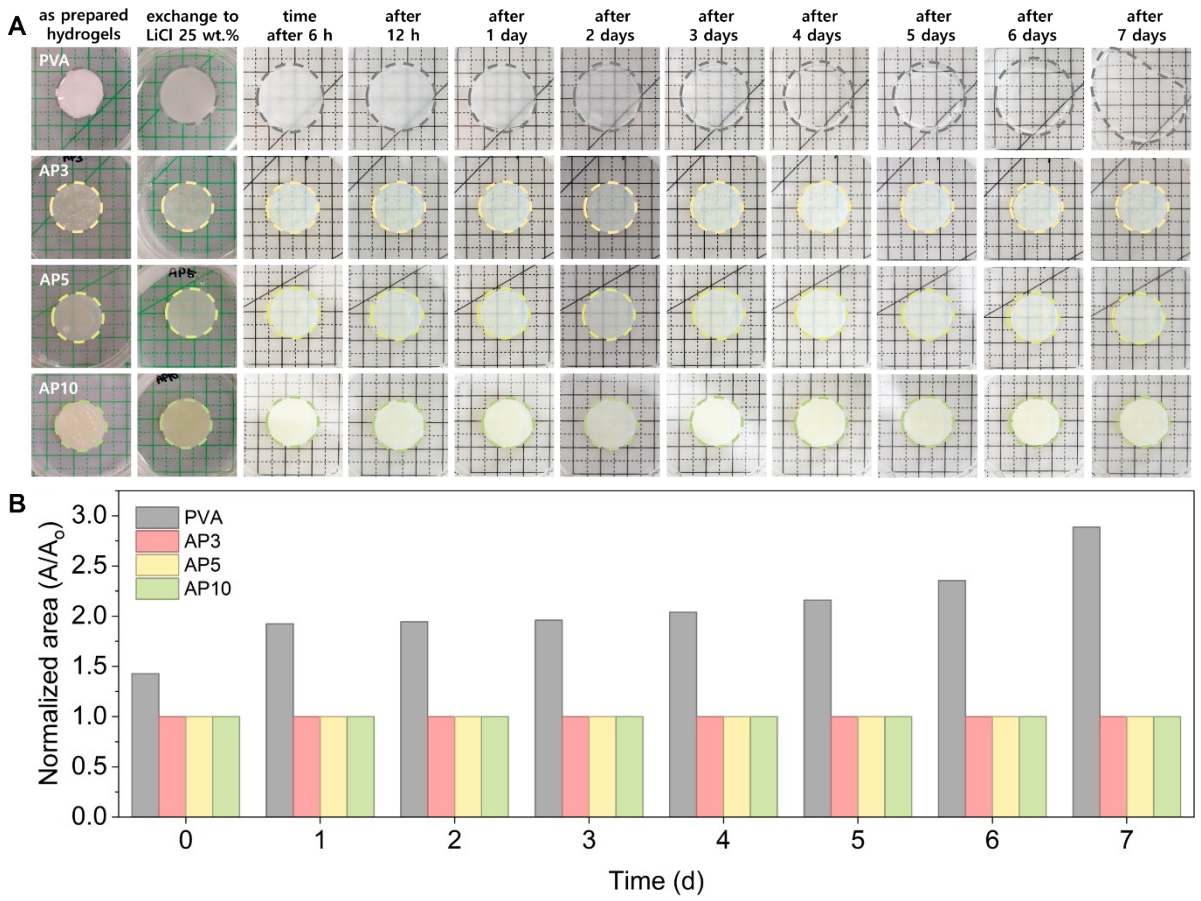

Figure S1. (A) Photographs of the as-prepared PVA and ANF-PVA hydrogel samples and their shape evolution after solvent exchange with LiCl aqueous electrolyte over time. (B) Time-dependent change in normalized area (A/A_0) relative to the initial sample area (A_0).

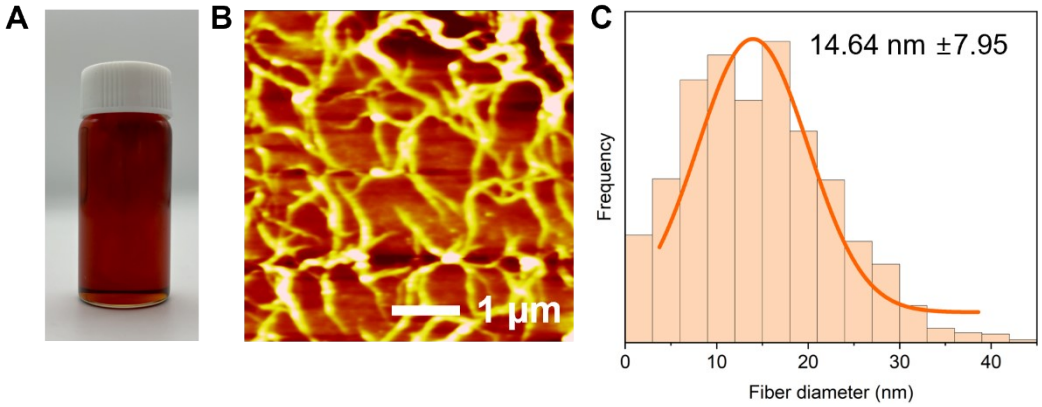

Figure S2. (A) Digital image of the ANF dispersion, (B) AFM image of the ANFs, and (C) average diameter and standard deviation of the ANFs determined from AFM image analysis.

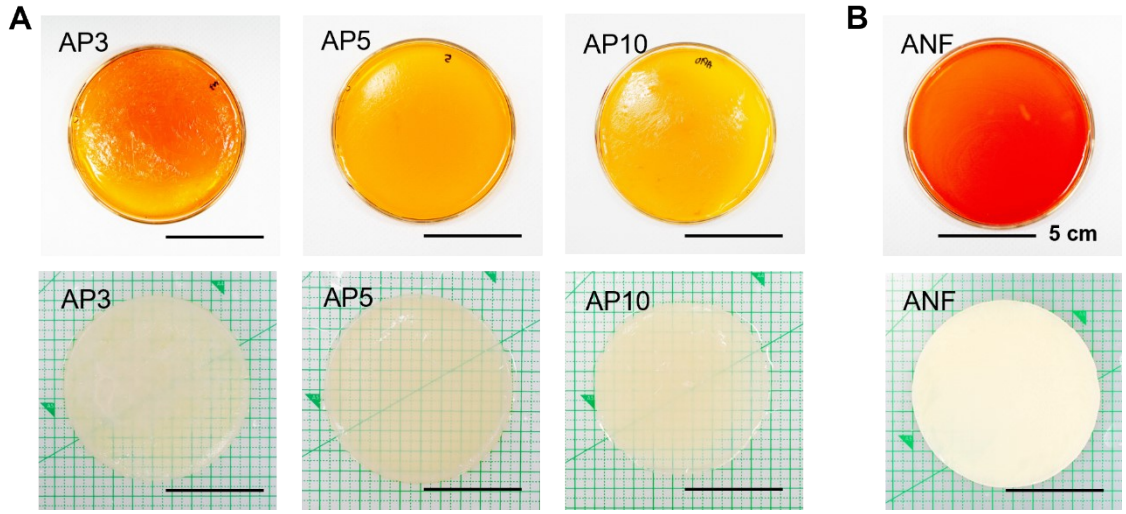

Figure S3. (A) Digital images of the ANF/PVA hydrogels with different compositions and (B) the ANF hydrogel, recorded prior to (upper panels) and following (lower panels) the reprotonation process.

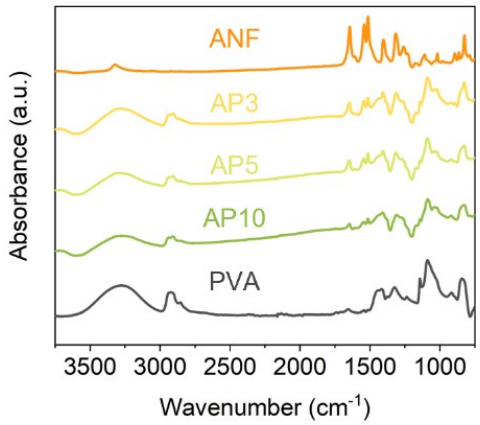

Figure S4. Full FT-IR spectra of the ANF hydrogel, the PVA hydrogel, and the AP hydrogels (AP3, AP5, and AP10).

	T_1 (°C)	T_2 (°C)	T_3 (°C)	T_4 (°C)	$M_{800°C}$ (%)
ANF	-	-	-	543	35.30
AP3	274	346	432	542	9.52
AP5	265	348	433	541	8.81
AP10	261	354	435	541	3.01
PVA	256	361	436	-	2.56

Table S1. Summary of decomposition peak temperatures (T_1–T_4) and residual mass at 800 °C ($M_{800°C}$) for ANF, PVA, and AP hydrogels obtained from TG/DTG analysis

	C (wt.%)	N (wt.%)	O (wt.%)
ANF	55.2 (3.39)	17.49 (0.54)	27.31 (2.87)
AP3	45.18 (3.03)	15.42 (0.51)	39.26 (1.81)
AP5	46.015 (1.66)	13.85 (0.85)	40.14 (1.75)
AP10	47.93 (1.51)	6.96 (0.59)	45.11 (0.92)
PVA	50.12 (3.30)	-	49.86 (3.30)

Values in brackets are standard deviation

Table S2. Summary of elemental weight fractions obtained from EDS analysis for ANF, PVA, and ANF/PVA composite (AP3, AP5, and AP10).

	Tensile strength (kPa)	Young's modulus (kPa)	Fracture strain (%)	Toughness (MJ m^{-3})
ANF	188.72 (1.93)	339.33 (11.01)	48.47 (0.68)	0.0429 (0.004)
AP3	160.62 (0.15)	106.67 (5.74)	136.27 (6.57)	0.102 (0.010)
AP5	539.27 (75.72)	75.67 (15.04)	386.67 (24.50)	0.92 (0.188)
AP10	316.47 (31.14)	10.03 (1.374)	960.1 (115.79)	0.86 (0.123)

Values in brackets are standard deviation

Table S3. Tensile strength, Young's modulus, and toughness of ANF and ANF/PVA hydrogels obtained from uniaxial tensile testing.

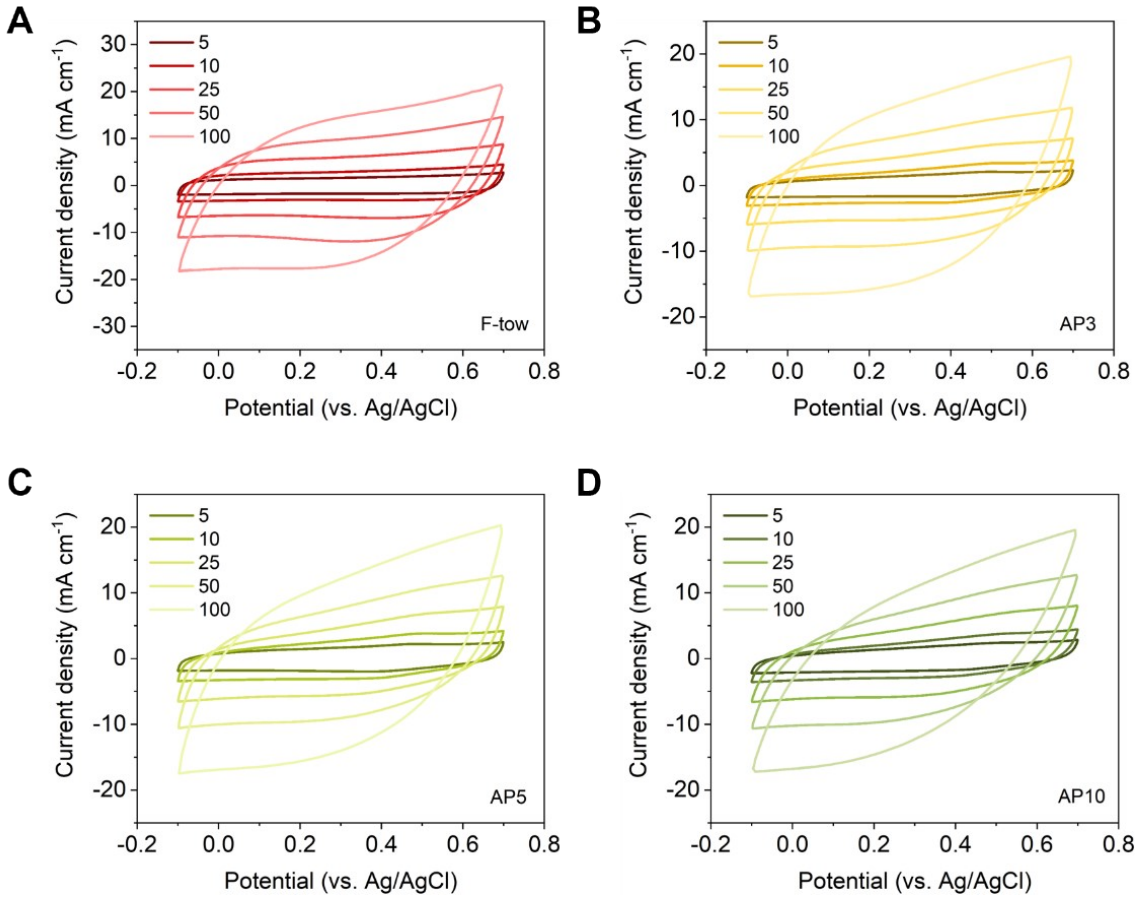

Figure S5. Full set of CV diagrams for (A) F-tow, (B) AP3, (C) AP5, and AP10 collected at scan rates of 5, 10, 25, 50, and 100 mV s^{-1}.

	Lap shear strength (kPa)	Lap shear stiffness (kPa mm^{-1})	Fracture energy (J m^{-2})
ANF	20.01 (0.81)	40.93 (7.59)	14.39 (2.15)
AP3	16.56 (0.23)	30.15 (4.83)	12.56 (0.92)
AP5	20.84 (2.19)	41.13 (0.45)	37.87 (1.77)
AP10	6.71 (0.13)	16.71 (2.38)	20.56 (2.77)

Values in brackets are standard deviation

Table S4. Mechanical adhesion parameters obtained from lap-shear testing

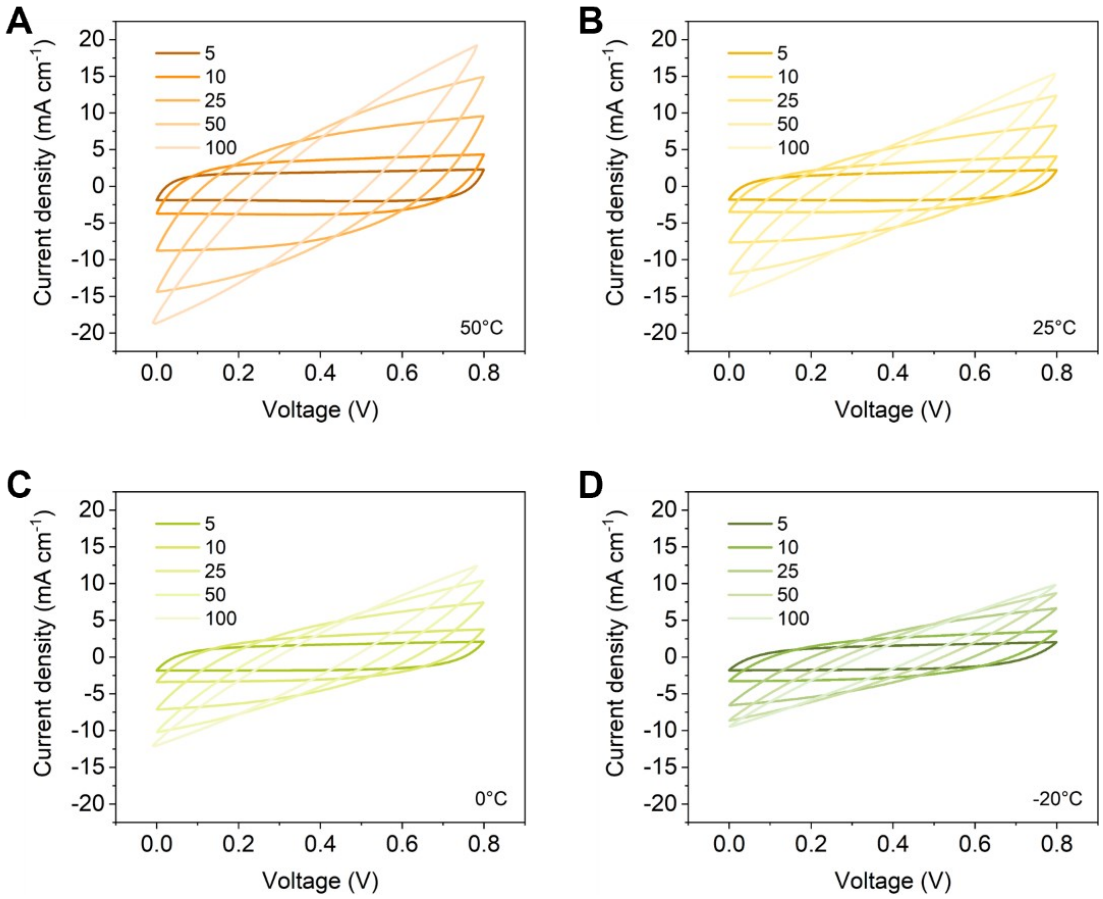

Figure S6. CV curves of the fiber-shaped supercapacitor measured at scan rates of 5, 10, 25, 50, and 100 mV s^{-1} under different temperature conditions (A) 50°C, (B) 25°C, (C) 0°C, and (D) −20°C.

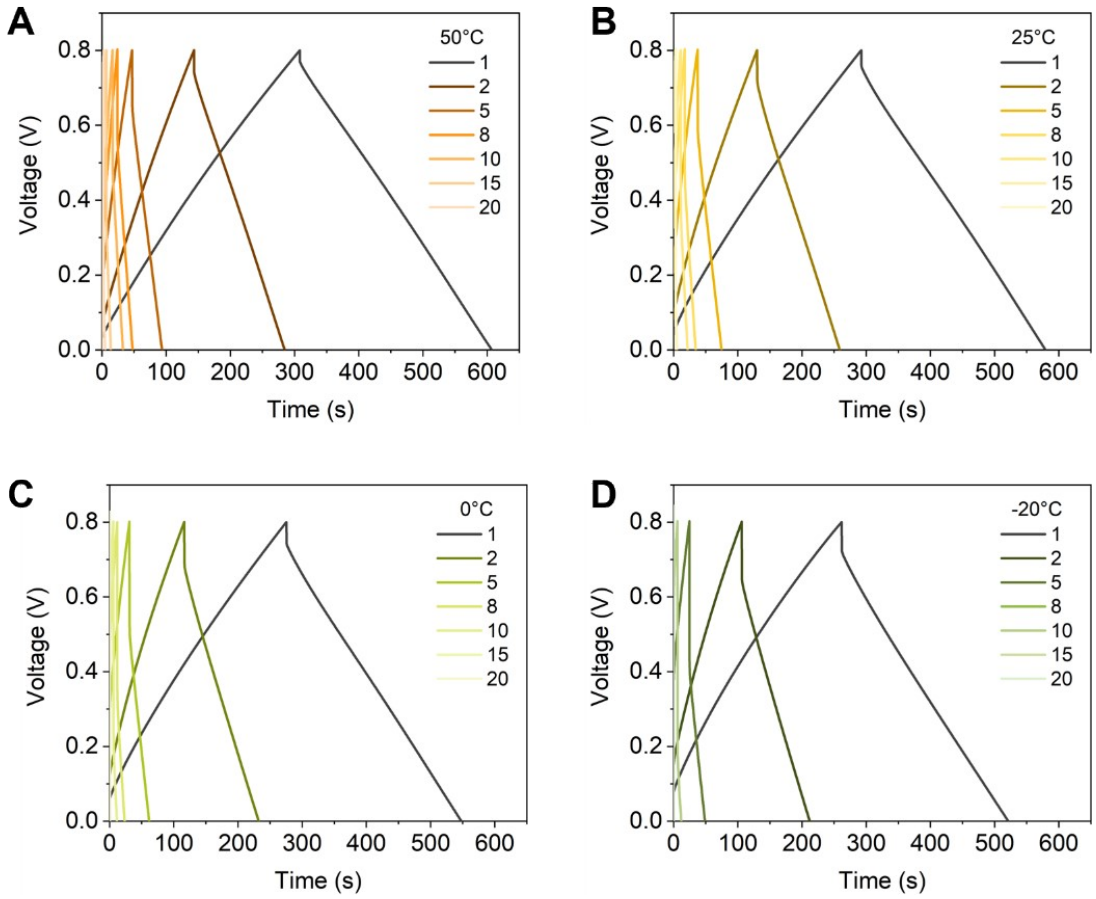

Figure S7. GCD curves of the fiber-shaped supercapacitor measured at different current densities (1–20 mA cm^{-1}) under various temperature conditions (A) 50°C, (B) 25°C, (C) 0°C, and (D) −20°C.

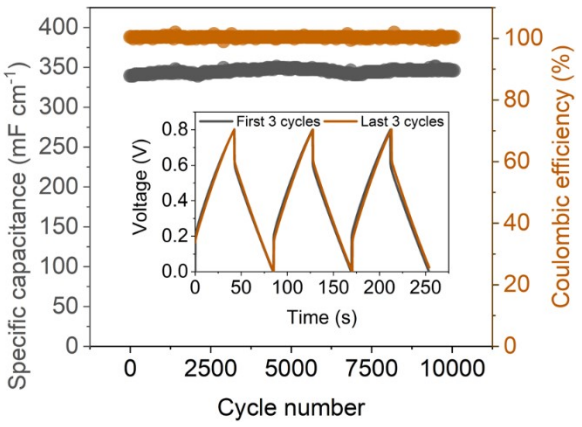

Figure S8. Cycling stability of the fiber-shaped supercapacitor at room temperature for up to 10,000 charge–discharge cycles.

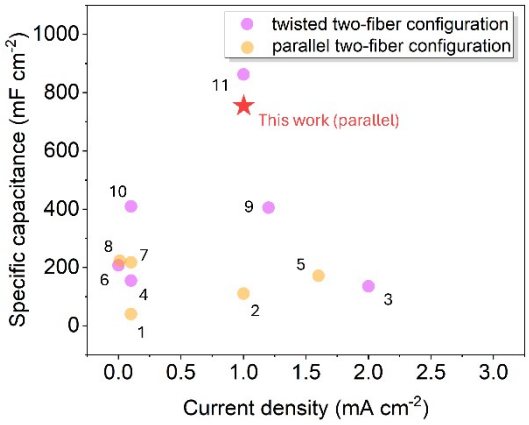

Figure S9. Comparison of areal specific capacitance of the present AP GPE–based fiber-shaped supercapacitor with previously reported fiber-shaped supercapacitors.

Electrode	Current density (mA cm^{-2})	Specific capacitance (mF cm^{-2})	Structure	Ref.
TiC_2T_x	0.1	41	Twisted	[1]
CMC//AC@CF	1	111	Twisted	[2]
c-ZIF-8@PF-0.20	2	136	Parallel	[3]
PANI/MWCNT-rGO/TPU	0.1	155.5	Parallel	[4]
MnO_2//rGO	1.6	172	Twisted	[5]
MnO_2//rGO@PPy	-	207.7	Parallel	[6]
CNFs-rGO/PPy	0.1	218	Twisted	[7]
Surface modified CF	0.01	223.6	Twisted	[8]
MoS_2/PEDOT:PSS/rGO	1.2	405.6	Parallel	[9]
MnO_2@ACF	0.1	410	Parallel	[10]
PMO-PGF	1	862.72	Parallel	[11]

Table S5. Tabulated areal specific capacitance data used for the comparison in Figure S9.

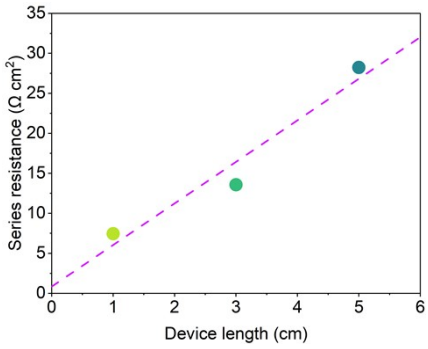

Figure S10. Series resistance as a function of device length for fiber-shaped supercapacitors. Linear extrapolation gives a finite intercept of ~0.841 Ω at zero length, attributed to contact and instrumental resistances. The slope or the series resistance normalized by device length was estimated as being 5.195 Ω cm^{-1}, confirming effective longitudinal scalability of the device.

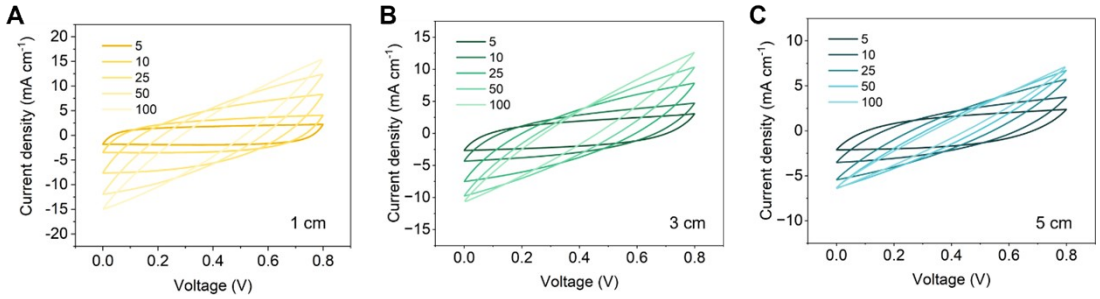

Figure S11. CV curves of fiber-shaped supercapacitors with different electrode lengths of (A) 1 cm, (B) 3 cm, and (C) 5 cm, measured at scan rates of 5, 10, 25, 50, and 100 mV s^{-1}.

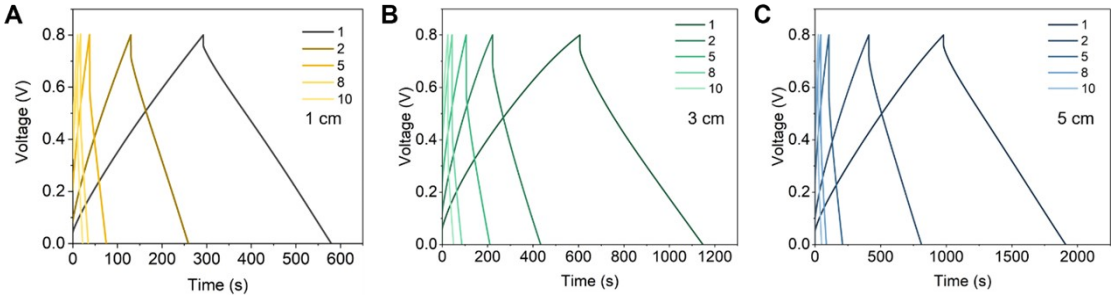

Figure S12. GCD curves of fiber-shaped supercapacitors with different electrode lengths of (A) 1 cm, (B) 3 cm, and (C) 5 cm, measured at currents of 1, 2, 5, 8, and 10 mA.

References

1. F. Ma, L. Li, C. Jia, X. He, Q. Li, J. Sun, R. Jiang, Z. Lei and Z.-H. Liu, *Journal of Colloid and Interface Science*, 2023, **643**, 92-101.
2. X. Lu, Y. Bai, R. Wang and J. Sun, *Journal of Materials Chemistry A*, 2016, **4**, 18164-18173.
3. X. Li, Y. Liu, M. Gao, X. Zhao and K. Cai, *Journal of Power Sources*, 2023, **580**, 233455.
4. Y. L. Tong, B. Xu, X. F. Du, H. Y. Cheng, C. F. Wang, G. Wu and S. Chen, *Macromolecular Materials and Engineering*, 2018, **303**, 1700664.
5. C. Choi, J. W. Park, K. J. Kim, D. W. Lee, M. J. De Andrade, S. H. Kim, S. Gambhir, G. M. Spinks, R. H. Baughman and S. J. Kim, *RSC advances*, 2018, **8**, 13112-13120.
6. N. Yu, Y. Li, L. Wang, X. Wang, Z. Sun, Z. Li, J. Luo, M. Cao and K. Guo, *Materials Today Energy*, 2021, **21**, 100758.
7. M. Mo, C. Chen, H. Gao, M. Chen and D. Li, *Electrochimica Acta*, 2018, **269**, 11-20.
8. Y.-G. Lee and G.-H. An, *Korean Journal of Materials Research*, 2022, **32**, 107-113.
9. Q. Zhou, G. Lv, X. Wang, W. Teng, P. Hu, Y. Du, H. Li, Y. Hu, W. Liu and J. Wang, *ACS Applied Energy Materials*, 2023, **6**, 5797-5805.
10. H. Li, J. Liang, H. Li, X. Zheng, Y. Tao, Z.-H. Huang and Q.-H. Yang, *Journal of energy chemistry*, 2019, **31**, 95-100.
11. G. Wu, Z. Ma, X. Wu, X. Zhu, Z. Man, W. Lu and J. Xu, *Angewandte Chemie International Edition*, 2022, **61**, e202203765.